



Targeting *Pdzn3* maintains adult blood-brain barrier and central nervous system homeostasis

Journal of Cerebral Blood Flow & Metabolism
2022, Vol. 42(4) 613–629
© The Author(s) 2021
Article reuse guidelines:
sagepub.com/journals-permissions
DOI: 10.1177/0271678X211048981
journals.sagepub.com/home/jcbfm



Florian Gueniot¹, Sebastien Rubin¹, Pauline Bougaran¹, Alice Abelanet¹, Jean Luc Morel² , Bruno Bontempi², Carole Proust¹, Pascale Dufourcq^{1,3}, Thierry Couffinhall^{1,4,*} and Cecile Dupl  a^{1,*} 

Abstract

Blood brain barrier (BBB) disruption is a critical component of the pathophysiology of cognitive impairment of vascular etiology (VCI) and associated with Alzheimer's disease (AD). The Wnt pathway plays a crucial role in BBB maintenance, but there is limited data on its role in cognitive pathologies. The E3 ubiquitin ligase PDZRN3 is a regulator of the Wnt pathway. In a murine model of VCI, overexpressing *Pdzn3* in endothelial cell (EC) exacerbated BBB hyperpermeability and accelerated cognitive decline. We extended these observations, in both VCI and AD models, showing that EC-specific depletion of *Pdzn3*, reinforced the BBB, with a decrease in vascular permeability and a subsequent spare in cognitive decline. We found that in cerebral vessels, *Pdzn3* depletion protects against AD-induced Wnt target gene alterations and enhances endothelial tight junctional proteins. Our results provide evidence that Wnt signaling could be a molecular link regulating BBB integrity and cognitive decline under VCI and AD pathologies.

Keywords

Vascular cognitive impairment, blood brain barrier, vascular permeability, Wnt pathway, endothelial tight junction

Received 24 February 2021; Revised 20 August 2021; Accepted 24 August 2021

Introduction

Cognitive impairment associated with aging has emerged as one of the major public health challenges of our time. Although Alzheimer's disease (AD) is the leading cause of clinically diagnosed dementia in Western countries, cognitive impairment of vascular etiology (VCI) and its severe form, vascular dementia, are the second most common cause.^{1,2} There is evidence that vascular dysfunction and blood brain barrier (BBB) disruption are critical components of the pathophysiology of VCI and are also increasingly recognized to be associated with AD.^{3–6} They develop as an early pathological event in pre-symptomatic individuals at risk for in VCI and AD.^{7–10} However, causal involvement of vascular mechanisms in the pathobiology of these diseases is still poorly understood.

In the central nervous system, the BBB is characterized by specialized endothelial cells (EC) with continuous intercellular tight junctions, that lack of

fenestration and have low rates of transcytosis, which greatly limits both the paracellular and transcellular movement of molecules through the EC layer.¹¹ Maintenance of BBB integrity is crucial for selective metabolic control of the brain interstitial fluid composition which is essential for proper synaptic functioning

¹Biology of Cardiovascular Diseases, University of Bordeaux U1034, Bordeaux, France

²Univ. Bordeaux, CNRS, IMN, UMR 5293, Bordeaux, France

³Service de Biochimie clinique, CHU de Bordeaux, Bordeaux, France

⁴Service des Maladies cardiaques et vasculaires, CHU de Bordeaux, Bordeaux, France

*These authors contributed equally to this work.

Corresponding author:

Cecile Dupl  a, InsermU1034, 1 avenue de Magellan, 33604 PESSAC.
Email: cecile.dupl  a@inserm.fr

and neuronal connectivity. When these junctions are disrupted, the barrier function is compromised and edema occurs, which can initiate pathways of neurodegeneration. Thus, great interest arises to delineate the signaling pathways regulating the physiological functions of the BBB and gain insights into the pathological conditions causing loss or breakdown of the BBB.

Among these, the canonical Wnt pathway, also known as Wnt/ β -catenin signaling, has been identified as playing a crucial role in the BBB development, maturation^{12–17} and phenotype maintenance.^{16,18} Transcriptomic analysis assessed that the most prominent up-regulated pathways in brain endothelial cells were the “Wnt signaling” and “adherens junction” pathways.¹⁹ We have reported that the E3 ubiquitin ligase PDZ domain-containing ring finger 3 (PDZRN3) was a mediator of the non-canonical Wnt pathway in EC. We have previously shown that during mouse development, endothelial specific *Pdzn3* overexpression causes early embryonic death due to brain hemorrhages²⁰ and that when *Pdzn3* is knocked out in EC, adult mice have reduced brain oedema in response to experimentally induced ischemic stroke.²¹

In this study, we investigated whether increase endothelial BBB dysfunction contributes to cognitive decline and degenerative processes. In order to tackle this question, a pathological mouse model was set up which replicate chronic cerebral hypoperfusion, induced by a gradual bilateral common carotid artery stenosis (GCAS). This GCAS model has previously been shown to produce white matter lesions, lacunar infarcts, hemorrhages, brain atrophy, and memory impairment in rodents.^{22,23} We applied GCAS to a transgenic model with a conditional EC-specific expression of *Pdzn3* (*Pdzn3*^{iECOE}) in adult. Under GCAS, *Pdzn3*^{iECOE} mice displayed an accelerated cognitive decline with an increase of brain tissue damage, an exacerbated BBB hyperpermeability. Conversely, EC depletion of *Pdzn3*, under GCAS, has a protective role against endothelial barrier leaks with an increase in endothelial tight junction protein levels. In a model of AD, deletion of *Pdzn3* in EC delayed cognitive decline with a decrease in vascular permeability, that limited neuron loss, glial reactivity.

In conclusion, we provide evidence of a molecular link between *Pdzn3* and maintenance of BBB integrity and subsequent cognitive decline under VCI and AD pathologies.

Materials and methods

Animals

Animal experiments were performed in accordance with the guidelines from Directive 2010/63/EU of the

European Parliament on the protection of animals used for scientific purposes and approved by the local Animal Care and Use Committee of the Bordeaux University CEEA50 (IACUC protocol #11656). General surgical procedures were conducted in mice (age 3–12 months, weight 25–35 g) according to ARRIVE guidelines (<https://www.nc3rs.org.uk/arrive-guidelines>).²⁴

To generate the inducible endothelial *Pdzn3* expression model, a triple transgenic strategy was employed and we followed the following breeding scheme. First we crossed *Pdgfb-iCre*^{ERT2} male mice²⁵ with female mice carrying *ROSA:LNL:tTA* (Jackson laboratory n° 011008) for Cre dependent expression of tTA. We backcrossed them to obtain *Pdgfb-iCre*^{ERT2} on homozygous *ROSA:LNL:tTA* background. The same strategy was employed to generate bi-transgenic mutant that has inducible expression of PDZRN3-V5 and beta-galactosidase (TRE-*Pdzn3-V5*) (generated previously)²¹ on homozygous *ROSA:LNL:tTA* background. *Pdgfb-iCre*^{ERT2}; *ROSA:LNL:tTA* male were then bred with *LacZ:Tre:Pdzn3-V5*; *ROSA:LNL:tTA* female to generate *Pdgfb-iCre*^{ERT2}; *ROSA:LNL:tTA*; *LacZ:Tre:Pdzn3-V5* (*Pdzn3* iECOE) and their littermates control, *ROSA:LNL:tTA*; *LacZ:Tre:Pdzn3-V5*. The expression of the tTA, which is dependent on the presence of Cre recombinase, induces the activation of either *Pdzn3-V5* and the reporter *LacZ* transgene to test for transactivation *in vivo*. Males and females from both lines were used for breeding and to maintain the colony. For endothelial cell-specific deletion, *Pdgfb-iCre Pdzn3*^{fl/fl} was generated previously.²¹ To generate Alzheimer's model, male transgenic mice heterozygous for the APP_{Sw} mutations (K670N/M671L driven by the prion protein promoter) in the human APP gene (Tg2576 line) (APP/PS1) were maintained on *Pdzn3*^{fllox/fllox} background by crossing APP/PS1 male with *Pdzn3*^{fllox/fllox} transgenic female. Then, *Pdgfb-iCre*^{ERT2}; *Pdzn3*^{fl/fl} male were bred with APP/PS1; *Pdzn3*^{fl/fl} female to obtain 4 groups: non dementia mutants *Pdgfb-iCre*^{ERT2}; *Pdzn3*^{fl/fl} (ND-iECKO) and their control group *Pdzn3*^{fl/fl} mice (ND-Litt) and APP/PS1 mutants APP/PS1; *Pdgfb-iCre*^{ERT2}; *Pdzn3*^{fl/fl} (APP/PS1; iECKO) and their control group APP/PS1; *Pdzn3*^{fl/fl} mice (APP/PS1; Litt).

For gene deletion or induction in adults (6–8 weeks), 0.5 mg of Tamoxifen (dissolved in an ethanol:sunflower seed oil mixture at 1:10 vol:vol) was injected intraperitoneally for four successive days.

Ameroid constrictor surgery

Ameroid Constrictor (AC) consists of a titanium casing surrounding a hygroscopic casein material with an inner diameter of 0.5 mm (Research Instruments SW,

CA, USA). Mice were anesthetized with a ketamine (100 mg/kg)/xylazine (20 mg/kg) combination and a neck incision was made and ACs are implanted surgically on bilateral exposed CCAs, free from their sheaths. To reduce the mortality rate after the surgery, the mice were kept in groups of only 2 mice per cage to decrease the risk of aggression. Hydrated food powders were poured into a bowl in the cage to avoid neck extension and the cages were partially changed during the experiment to avoid any manipulation of mice. Cerebral blood flow was measured with a laser-doppler imager (MOORLDI2-IR, Moor instrument) before and after surgery.

Immunohistochemistry

Mice were anesthetized with sodium pentobarbital (120 mg/kg, i.p.) and perfused transcardially with PBS followed by 4% paraformaldehyde (PFA) in PBS and brains were removed and split into hemispheres which were post-fixed in 4% PFA at 4°C for 3 h to be either embedded in paraffin or in OCT for brain freezing.

Histological stains

Paraffin embedded brains were sagittally sectioned at 7 µm and sections for the following staining, Haematoxylin and eosin staining and Perl's staining.

Each hemisphere was entirely cut and 2 adjacent sections each 100 µm (16 sections in total) were analyzed per animal per condition. Bright-field images were acquired using slide scanned images, allowing us to analyze entire sections instead of a random selection of fields (slide scanner nano zoomer Hamamatsu). Ischemic and bleed area and number were delineated manually and quantified using ImageJ software. All the data were pooled for each hemisphere.

Immunostaining of mouse tissue

Frozen hemispheres were sagittally sectioned using a cryotome at 20 µm. Immunostaining was performed as previously described²¹ with primary antibodies β galactosidase (1:500, Abcam, ab9361), Albumin (1/200, Abcam, Ab8940), Fibrinogen (1:500; Dako; A0080), GFAP (1:400, Thermofisher, 1-06100), laminin (1:400, Dako, Z0097), NeuN (1:400, Merck, ABN78), Iba-1 (1:200, Wako, 019-19741) Podocalyxin (1:300, R&D, AF1556), in blocking solution overnight at 4°C before being incubated with Alexa Fluor secondary antibodies (1:400, Invitrogen) for 4 h at room temperature. Sections were washed in PBS (3 × 5 min), incubated with Hoechst 33342 (Invitrogen).

Fluorescent images were acquired either using Zeiss AxioZoom V16 stereo microscope or Zeiss LSM700 confocal laser-scanning microscope. Confocal images

were analyzed with Bitplane software (Imaris). Three-dimensional projections were digitally reconstituted from stacks of confocal optical slices by Zeiss software (Carl Zeiss Microimaging). Image post analysis was performed using ImageJ software.

Quantification: for each animal, at least 2 × 2 non adjacent sections (>100 µm apart) were analyzed per animal per condition. For NeuN+ neuronal, GFAP+ astrocyte and Iba1+ section quantification, either all the cortex or the CA1 (Hoechst +) stained area were delineated manually. For extravascular leakages, where possible, fibrinogen and IgG extravasations were analyzed on the entire cortical or hippocampal areas and quantified using a semi-automated method. Stained area was quantified using a semi-automated method using ImageJ software. The experimenter was blinded to the genotype throughout quantifications which were carried out manually.

Capillary isolation

Mice were transcardially perfused under deep anesthesia (pentobarbital 300 mg/kg) with 30 ml of heparinized saline to remove blood cells. Brain were isolated and cerebellum, olfactory bulbs and meninges were removed from the brain. The brains were subsequently homogenized as described.²⁶ Briefly, capillaries were isolated using dextran gradient centrifugation to remove myelin fat, followed by a first filtration on a 100 µm filter to remove large fragments then a filtration on 20 µm filter (Millipore). The isolated capillaries were collected in PBS and either lysed for immunoblot or RT-qPCR analysis or were prefixed in PFA 4% during 5 min for immunolabeling.

Four subcellular fractions including cytosolic, membrane, nuclear, and cytoskeletal fractions were prepared from brain microvessels by using the ProteoExtract[®] Subcellular Proteome Extraction Kit (Merk Millipore) according to the manufacturer's instructions. (see details in *SI Materials and Methods*).

For immunofluorescent Ve-cadherin and Claudin5 junction analysis in capillaries, SMA+ arterioles were excluded and 12 µm maximum projection z-stack images were reconstructed. Between both adjacent endothelial nuclei, line scan analyses were performed using Fiji and intensity of fluorescence at the endothelial cell-cell junction was quantified using a semi-automated method as reported.²⁷ Antibodies used were Ve-cadherin (1:400, R&D, AF1002), Claudin5 (1:400, Millipore, ABT45), SMA (1:1000, Sigma, C6198) .

RNA preparation and quantitative PCR

Mouse tissues were homogenized in Tri-reagent[™] (Sigma) and RNA was extracted according to the

manufacturer's instructions. Quantitative real time RT-PCR (qRT-PCR) were performed as described previously.²¹

(see details in *SI Materials and Methods*).

Western blot

Cell lysates were resolved by SDS-PAGE and probed with indicated antibodies (see details in *SI Materials and Methods*).

Behavioral tests

Visual behavior testing. mice underwent visual behavior testing one day before the y-maze test using a visual cliff test reported in supplementary file.

Modified Y-maze testing: during the training phase, one arm was blocked by a removable door. In this phase the mice were positioned in the start arm, facing the center of the maze and allowed to explore only two arms (named "start" arm and "old" arm) for 5 min. The training protocol consisted of three 5 min bouts of exploration separated by 5 min rest periods. At the end of the training trial, 30 min later the door blocking the novel arm is removed and the animal were placed again in the start arm and allowed to explore the three arms ("start", "old" and "new" arms) during 5 min. The time spent in each arm was measured. All experimental data was analyzed using the video tracking system (Noldus EthovisionXT). The index of memory performance was calculated as a ratio of (time spent in "new" arm – time spent in "old" arm)/(time in "new" arm + time in "old" arm).

Nesting test was reported in supplementary file as described.²⁸

Statistics

Data are represented as individual values plus means \pm SD. The sample size, what each "n" represents, the statistical tests used and the result of the statistical test are indicated in each respective figure legend. Statistical analyses were performed using Prism v8.0 (GraphPad) software. Differences between two different groups (either age or genotype) were analyzed by unpaired t test. Differences among different genotype groups were analyzed by one-way ANOVA followed by a Bonferoni's multiple comparisons correction. Differences among different age groups and genotype were analyzed by two-way ANOVA followed by a Bonferoni's multiple comparisons correction. Normality and equality of variances among the groups were analyzed by Brown-Forsythe tests. P values less than 0.05 were considered significant.

Results

Vascular endothelial specific Pdzrn3 overexpression leads to enhance brain damage and cognitive defects after gradual carotid artery stenosis

It was shown experimentally that chronic cerebral hypoperfusion induced BBB breakdown and an increase in vascular permeability²⁹. We wanted here to test if BBB breakdown under hypoperfusion may worsen cognitive impairment.

To test this hypothesis, we developed a mouse model with an endothelial specific ectopic overexpression of *Pdzrn3* (iECO). In order to overexpress *Pdzrn3* conditionally in vascular EC, we crossed *Pdgfb* iCre^{ERT2}²⁵ with ROSA:LNL:tTA transgenic mice³⁰ to generate *Pdgfb*-iCre^{ERT2}/ROSA:LNL:tTA bigenic mice in which tTA was turned on specifically in EC. We then crossbred *Pdgfb*-iCre^{ERT2}/ROSA:LNL:tTA mice with *TRE*-*Pdzrn3* mice (expressing PDZRN3-V5 and β galactosidase when tetO was activated by tTA).²⁰ We obtained both groups: *Pdgfb*-iCre^{ERT2}/ROSA:LNL:tTA/tetO-*Pdzrn3* triple-transgenic mice (*Pdzrn3* iECO) and *Pdgfb*-CreER/ROSA:LNL:tTA (control group) (Figure 1(a)). As CNS vasculature undergoes angiogenesis and remodeling at early post-natal stages which may impact BBB function,³¹ we chose to induce *Pdzrn3* by Tamoxifen administration in adult mice (> 8 weeks). Our targeting design allowed following of recombination events using β -galactosidase staining. We reported that Cre-mediated recombination and EC expression of *LacZ* throughout the CNS in different brain regions as cortex, hypothalamus and cerebellum (Figure 1(b) to (c)). *Pdzrn3* iECO mice were viable and did not show any gross morphological abnormalities (data not shown). We did not find any modification of vessel organization in brain volumes in iECO mice vs littermates by light sheet microscopy (fig. S1(a) to (c)).

To investigate the functional outcomes associated with *Pdzrn3* OE, we prepared intact brain vessel fragments from the brain of control and *Pdzrn3* iECO mice, to preserve the BBB structural integrity and their molecular properties³² (Figure 1(d)). We analyzed the expression levels of BBB gene markers as *Cdh5* (Ve cadherin), *Cldn5* (claudin5) and *Ocln* (Occludin) and of Wnt target genes in brain vessel extracts. BBB gene markers were not differentially expressed (Figure 1(e)). Consistent with the role of *Pdzrn3* in inhibition of canonical Wnt signaling, we found a significant down regulation of *Axin2* in the iECO mutants but not of *Lef1*, *Nkd1* or *Gpr124* (Figure 1(e)). We further study whether *Cldn5*, *Cdh5* and *Ocln* were regulated at the protein levels; subcellular fractionation experiments were then performed on

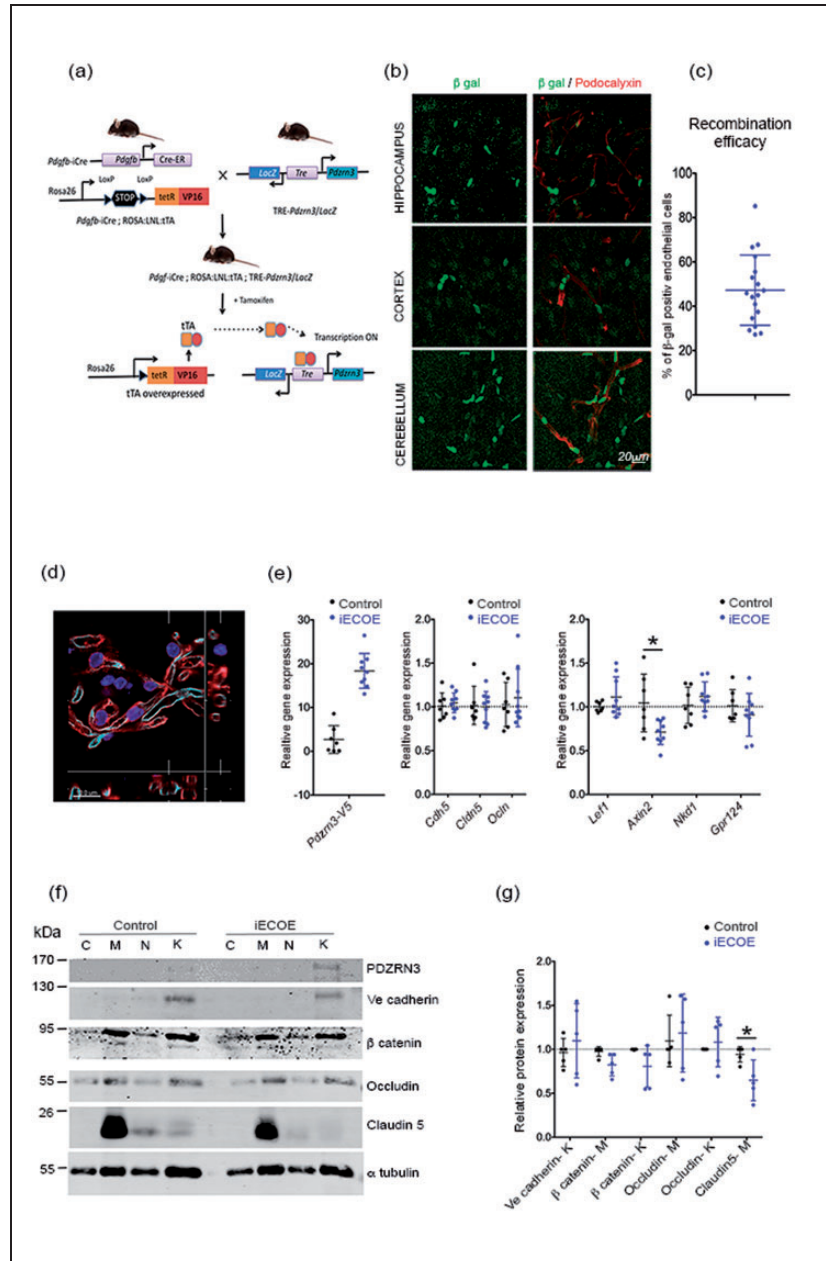


Figure 1. Overexpression of *Pdzrn3* (iECO) specifically in endothelial cells. (a) Cre mouse line for overexpression of *Pdzrn3* in EC: (A) Breeding scheme for the generation of a *Pdgfr-cre*/*Rosa*/*LNL:τTA*/*tet-Pdzrn3*; *LacZ* (*Pdzrn3* iECO) triple transgenic mouse (b) Confocal immunofluorescent images of β galactosidase expression (green) in podocalyxin labeled endothelial cells (red) in hippocampus, cortex and cerebellum sections of transgenic *Pdzrn3* iECO mice, revealing endothelial specific cre-mediated transgene activation. Scale bar = 20 μ m. (c) Quantification of the number of podocalyxin positive ECs showing *Pdgfr-cre* recombination efficacy. (d) Vessel fragments were isolated from harvested mouse brain and immunolabeled with CD31 (red), Podocalyxin (light blue) and Dapi (blue). Scale bar = 10 μ m. (e) Vessel fragments were subjected to qRT-PCR. Representative immunoblot images (f) and quantification (g) of TJ proteins Occludin, Claudin5, AJ protein Ve cadherin and of β catenin in control and *Pdzrn3* iECO brain subcellular microvessel fractions: cytosol (C), Membrane (M), nucleus (N), cytoskeleton (K). n = 5. Data are represented as individual values plus means \pm SD. Mann-Whitney test was performed. *p < 0.05.

purified microvessels. PDZRN3 expression was detected in the cytoskeletal fractions; its expression was increased in fractions from *Pdzrn3* iECO (Figure 1(f)). Our results did not evidence changes in

localization of junction proteins in both groups. Ve cadherin was mainly detected in cytoskeletal fractions, Claudin5 in membrane fractions; Occludin is distributed in both membrane and cytoskeletal fractions,

β catenin levels in the different fractions was not modified. We observed a significant decrease of Claudin5 expression in membrane fractions of *Pdzn3* iECOE mutants compared with their respective littermate control but we did not detect significant difference in Ve cadherin and/or Occludin expression in respectively skeletal and in membrane fractions between both groups (Figure 1(f) to (g)).

An experimental model of VCI model was induced by ameroid constrictors implantation on both common carotid arteries. This model generated a slow gradual carotid artery stenosis (GCAS)^{22,23} (fig. S2 (a)) and as expected, induced a time-dependent gradual decrease in cortical brain cerebral blood flow (CBF) in iECOE mutants and controls (Figure 2(a)). We analyzed whether *Pdzn3* ectopic expression may enhance cognitive defects after GCAS. For this purpose, around 20–28 weeks old *Pdzn3* iECOE and littermate control groups, before and after surgery, underwent spatial recognition memory testing. A modified version of Y-maze two-trial arm discrimination paradigm was designed to increase cognitive demand. Mice underwent an acquisition phase consisting of 3 successive 5 minutes exploration sessions with only two accessible arms in the maze to maximize encoding. Subsequent the acquisition phase, the third arm was made accessible to facilitate the test phase. After an inter-trial interval of 30 minutes, this training regimen resulted in a robust preference for the unexplored (previously inaccessible) arm during the test phase (fig. S2 (b)).

Pdzn3 overexpression made iECOE mice hypersensitive to hypoperfusion which resulted in a high mortality rate 14 days after the onset of the model (Figure 2 (b)). To circumvent this issue, we evaluated cognitive performance at 7 days after GCAS, a delay which additionally enabled control mice to exhibit a higher level of memory performance compatible with the detection of impaired performance in iECOE mice, in both the control and *Pdzn3* iECOE groups. In the absence of a potential floor effect, we found spatial recognition memory performance of iECOE to worsen compared to their littermate controls (Figure 2(c)). Before surgery, *Pdzn3* iECOE mutant mice performed similarly to control mice (Figure 2(c)). We verified that iECOE mice displayed comparable locomotor activity and performed similarly to their control littermates when tested in the visual cliff paradigm thus attesting that visual perception and sensorimotor abilities were not compromised in these genetically-modified mice (fig. S3 (a) and (c)).

We next performed in-depth analyses of effect of the ectopic endothelial *Pdzn3* expression on brain lesions after GCAS surgery. At 14 days after surgery, GCAS in iECOE mice resulted in significant hippocampal neuronal loss in the CA1 hippocampal region as compared

to littermate known to play a supportive role in spatial recognition memory (Figure 2(d) to (e)). In the cortical region GCAS induced a reduced neuronal loss in both iECOE and their littermates (Fig S7 (a)). Astroglia is a hallmark of damaged brain tissue. Under normal conditions, astrocytes in mouse hippocampus and cortex usually express little GFAP.^{34–36} To study the dynamic change of reactive astrocyte generation, we have quantified hippocampal and cortical GFAP expression as a marker of reactive astrocytes. We found that GCAS induced an activation of astrocytes as already reported³⁷ and that iECOE amplified the level of GFAP activation (Figure 2(f) to (g), Fig S7 (b)).

Hematoxylin and eosin (H&E) and Perl's Prussian blue staining have been used to localize cerebral microinfarcts and microbleeds on the whole brain.³⁸ A significant increase in brain microinfarct lesions (Figure 2 (h) to (i)) and of large bleeds (Figure 2(j)) was quantified in the brain of iECOE mutant mice compared with controls (Fig S4 (a) and (b)).

Taken together, these data indicate that enhancement of PDZRN3 activity in ECs is highly correlated to cognitive loss as well the development of brain lesions and astrocyte activation after GCAS.

Vascular endothelial specific Pdzn3 overexpression leads to enhanced BBB leakage with altered expression of TJ proteins after gradual carotid artery stenosis

We then hypothesized that ectopic expression of *Pdzn3* enhances the BBB permeability. Prior to surgery, we noticed that mice with endothelial-specific overexpression of *Pdzn3* (iECOE) showed spontaneous discrete IgG extravasation surrounding arterioles and diffuse IgG extravasation in the cortex and hippocampal area, but this was not significantly different when compared to that in control mice (Figure 3(a)). Under GCAS at 14 days, fibrinogen and IgG extravasation into brain parenchyma in both the cortical and hippocampal area were strongly apparent in the *Pdzn3* iECOE group, suggesting that forced expression of *Pdzn3* results in major defects in the entire brain vasculature (Figure 3(a) to (e)).

To define the mechanism of action of PDZRN3 signaling in regulating BBB permeability, we analyzed whether induced endothelial expression of PDZRN3 may affect TJ and AJ proteins expression and/or distribution in extracted vessels after GCAS. At 10 days after GCAS, we reported a strong decrease of Claudin5 and Occludin expressions in vascular membrane fractions from *Pdzn3* iECOE mice compared with controls without significant alteration in Ve cadherin and β catenin expression levels. We did not show any significant

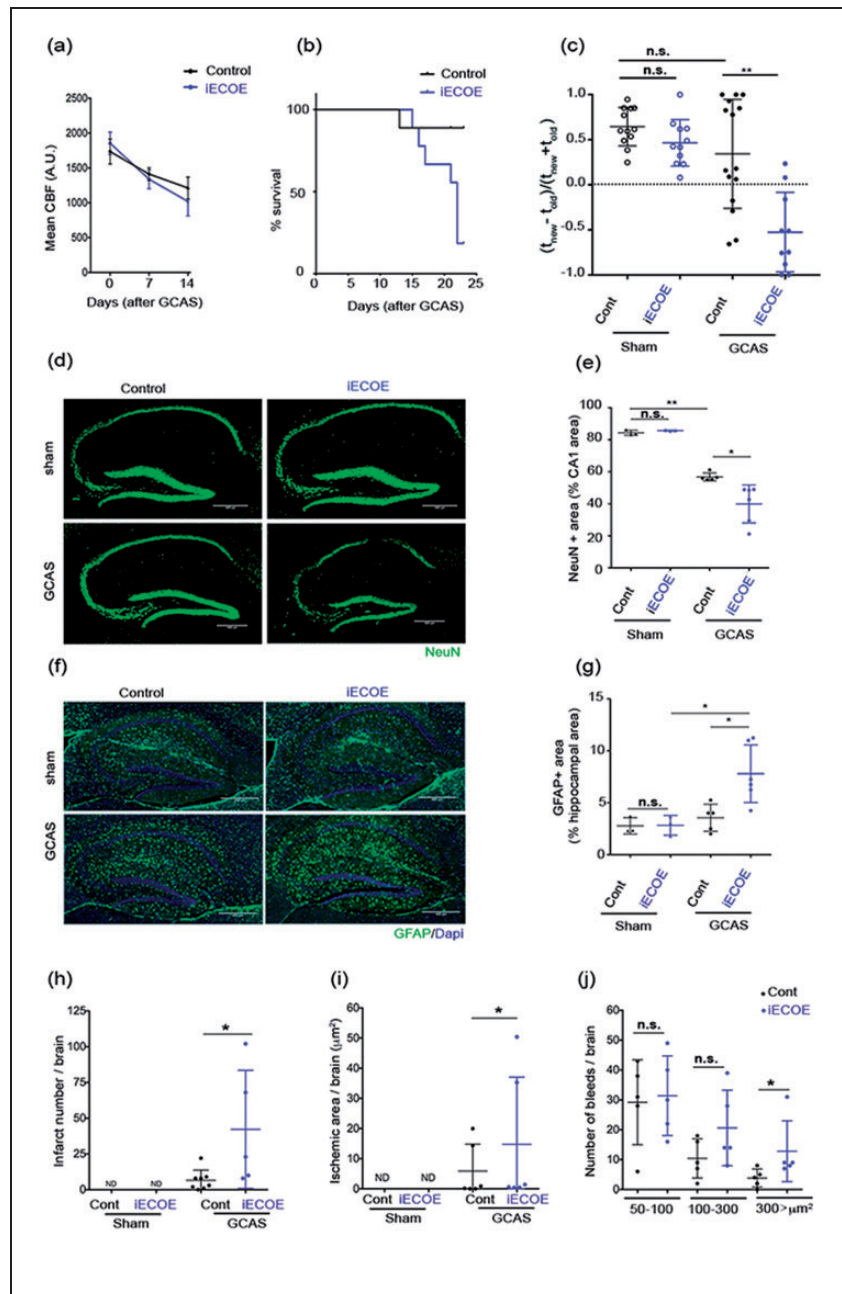


Figure 2. Endothelial overexpression of *Pdzrn3* enhances cognitive defects and brain damage after gradual carotid artery stenosis (GCAS). (a) Cerebral blood flow (CBF) decreases gradually in all groups (Control, *Pdzrn3* iECO mice) after implantation of ameroid constrictors (GCAS). Two groups were not significantly different in 2-way repeated-measures ANOVA from day 0 to day 14. ($n = 10$ per group). (b) Kaplan-Meier curve showing survival rate of control and *Pdzrn3* iECO (iECO) mice before and until 21 days after GCAS ($n = 10$ per group). (c) Y-maze exploration test: evaluation of cognitive performance in *Pdzrn3* iECO mice before (sham) and at 7 days after GCAS showing that endothelial *Pdzrn3* overexpression worsened the test. Data are represented as individual values plus means \pm SD. Significance was assessed by 2-way ANOVA. Each group contained 11–15 mice and each mouse is indicated as a dot in graphs. (d) Representative hippocampal immunofluorescent staining for NeuN before (Sham) and after GCAS at 21 days in control and iECO mice. (e) NeuN+ cells were quantified as a percentage of the area occupied in the CA1 area non-operated (sham) and after GCAS from iECO vs their respective control littermate mice. (f) Representative hippocampal immunohistochemical staining for GFAP before (Sham) and at 21 days after GCAS in control (Cont) and iECO mice. (g) GFAP were quantified in hippocampal area before and after GCAS in iECO mice versus their respective control littermates. Data shown in the graphs are obtained in sham condition, from 3 mice per group and in GCAS condition from $n = 6$ iECO vs $n = 5$ control mice; data for four brain slices per mouse were recorded and averaged to produce a single value for each mouse. One-way ANOVA was performed. Data are represented as individual values plus means \pm SD. Infarct number ($n = 8$ iECO vs $n = 5$ control) (h), ischemic area ($n = 6$ per group) (i) and bleed number ($n = 5$ per group) (j) were quantified in brains from either non operated (sham) or after 21 days of GCAS from control vs iECO mice. Data for eight brain slices per mouse were recorded and averaged to produce a single value for each mouse. One-way ANOVA was performed. Data are represented as individual values plus means \pm SD.

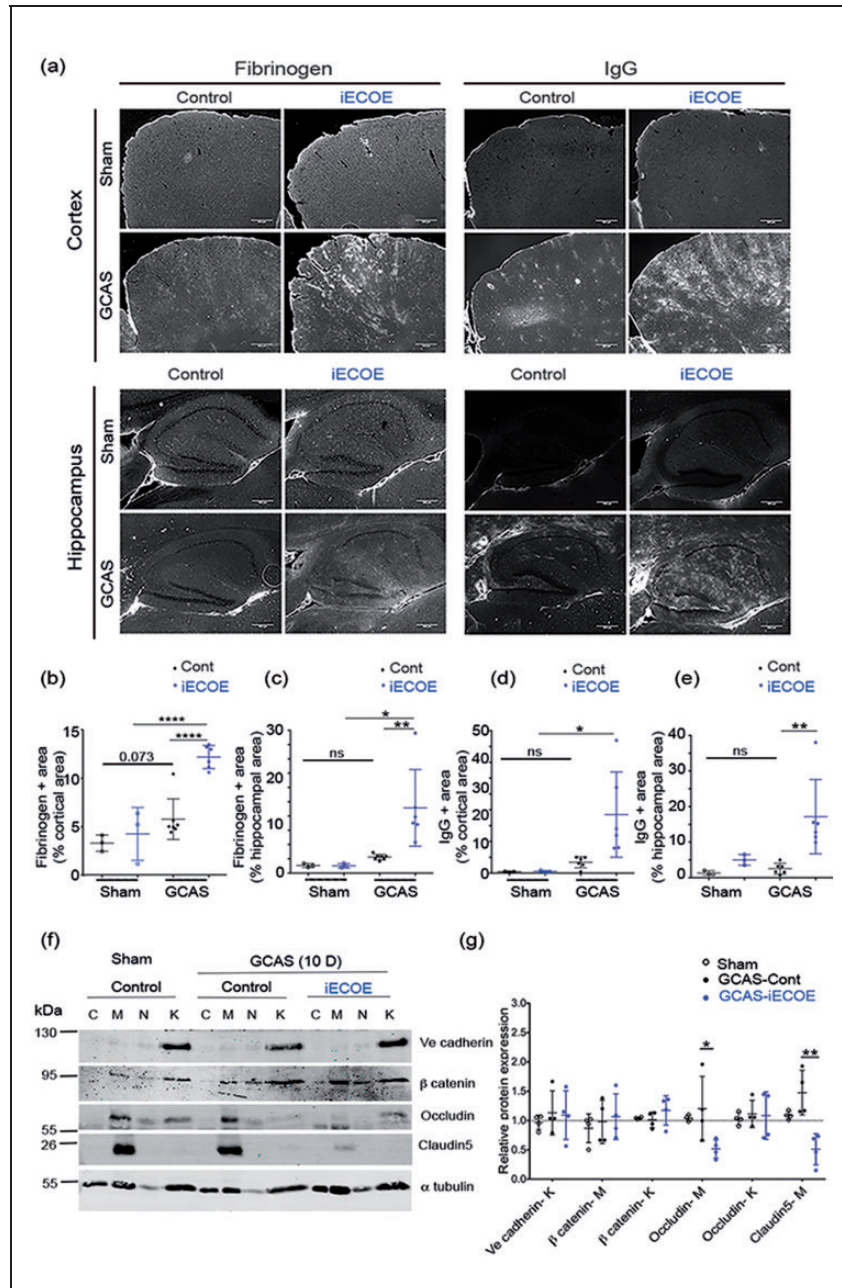


Figure 3. Endothelial *Pdzrn3* ectopic expression induces BBB leakage. (a) Representative image of Fibrinogen and IgG immunostaining in cortical and hippocampal regions, in non-operated (sham) brains and at day 14 after GCAS surgery, from control versus *Pdzrn3* iECOE mice. Scale bar represents 100 μ m. Fibrinogen (b–c) and IgG (d–e) was quantified as a percentage of the area occupied either in cortical region or in hippocampal region in non-operated (sham) and after GCAS brain sections. Quantification was done in brains from non operated (sham) control (n = 3) vs iECOE (n = 3) mice and in brains recovered after 14 days of GCAS from control (n = 7) vs iECOE (n = 6) mice and reported below. Data for two brain slices per mouse were recorded and averaged to produce a single value for each mouse. One-way ANOVA followed by Kruskal-Wallis test was performed. Data are represented as individual values plus means \pm SD. (f) Representative immunoblot images and (g) quantification of TJ proteins Occludin, Claudin5, AJ protein Ve cadherin and of β catenin in control and *Pdzrn3* iECOE brain subcellular microvessel fractions at 10 days after GCAS: cytosol (C), Membrane (M), nucleus (N), cytoskeleton (K). n = 4. Data are represented as mean \pm SD. Mann-Whitney test was performed.

*p < 0.05.

modification in their localization in the different fractions. (Figure 3(f) to (g)). These biochemical results suggest that ectopic expression of PDZRN3 signaling enhanced BBB leakage under GCAS through loss of endothelial TJ proteins at the endothelial membrane.

Endothelial-specific depletion of *Pdzrn3* protects against cognitive impairment, loss of neurons in hippocampal CA1 region and astrocyte activation after gradual carotid artery stenosis

Given that *Pdzrn3* function is linked with reduced endothelial integrity, we asked whether the cerebral phenotypes after GCAS could be rescued by repression of *Pdzrn3* expression in brain EC.

To repress *Pdzrn3* expression in EC, we crossed mice bearing a *Pdzrn3* flox allele (*Pdzrn3^{f/f}*) with an EC-specific *Pdgfb-Cre^{ERT2}* transgene to generate *Pdgfb-Cre^{ERT2}; Pdzrn3^{f/f}* (iECKO) and *Pdzrn3^{f/f}* littermates.²¹ To exclude any confounding effect of endothelial-specific *Pdzrn3* deletion on general microvessel organization in the CNS, we examined the vasculature in iECKO mice vs control littermates by light sheet microscopy throughout the brain volume and found no differences in vascular density across cortical areas between the two groups (fig. S1(a) to (c)). Constrictors were efficacious in inducing time-dependent graded hypoperfusion within 21 days with no difference between iECKO mice and littermates (Figure 4(a)) and with no effect on mouse survival (Figure 4(b)).

Pdzrn3 iECKO and littermate control groups then underwent spatial recognition memory testing by using the modified Y-maze two-trial arm discrimination paradigm (Fig. S2 (b)). While iECKO mice displayed a performance level similar to that of control littermate mice achieved prior and 7 days after surgery (Figure 4 (c)), a different memory profile emerged when mice were tested 10 days after undergoing surgery to induce VCI; their littermate controls had a lower level of performance, failing to discriminate the novel arm (unpaired t-test, $p = 0.0028$) (Figure 4(c)). Thus, endothelial-specific *Pdzrn3* deletion appears to protect the mice from disturbed spatial recognition memory induced by GCAS. This beneficial effect was memory-specific as there was no confounding effect of GCAS on the total exploration time of arms of the maze during either the encoding phase or the test phase (Fig. S3 (a) to (c)). Nesting was used as a complementary assay and showed that the quality of nests constructed by iECKO mutant mouse group, 10 days after GCAS, was significantly better than in control mouse group (Figure 4(d)). In addition, iECKO mice performed similar to their control littermates when tested in the visual cliff paradigm and displayed

comparable locomotor activity, thus attesting that visual perception and sensorimotor abilities were not modified in these genetically-modified mice (Fig. S3).

Brain lesions were analyzed after GCAS. Compared to controls, iECKO mice exhibited a reduced neuronal loss in the CA1 hippocampal region after GCAS (Figure 4(e) to (f)). GCAS induced a reduced neuronal loss also in the cortical region but no significant difference was found between iECKO and littermates before and after GCAS (Fig S8 (a)). To evaluate the effect of the endothelial-specific *Pdzrn3* on brain astrocyte activation, we quantified hippocampal and cortical GFAP expression. GCAS induced activation of astrocytes in both regions, an effect counteracted by the loss of *Pdzrn3* which decreased GFAP positive labelling in the hippocampus and in the cortex (Figure 4(g) to (h), Fig S8 (b)). We then reported a significant decrease in the number of brain lesions (Figure 4(i) to (j), fig. S5 (a)) but no significant differences in numbers or size of microbleeds between both groups were observed at 21 days after GCAS (Figure 4(k); fig. S5 (b)).

Reduced BBB breakdown in mice with endothelial-specific depletion of *Pdzrn3* (iECKO) after gradual carotid artery stenosis with enhanced expression levels of tight junction proteins

To analyze whether EC down regulation of *Pdzrn3* modulates BBB disruption after GCAS, total brain sections were triple stained for an endothelial cell marker (Podocalyxin), astrocytes (GFAP) and fibrinogen to assess blood extravasation across the BBB.

In control littermates, the GCAS model induced rupture of both endothelial and astrocyte layers with blood born molecule extravasation, while in *Pdzrn3*-deficient mice (iECKO), there was a significant reduction in BBB leakage, in the cortex and hippocampal regions (Figure 4(l), Fig S8 (c)). Reduced fibrinogen accumulation in hippocampus and IgG in cortex in iECKO compared to littermate was respectively quantified (Figure 4(m), Fig S8 (c)). We then asked whether endothelial *Pdzrn3* repression favored the maintenance of brain TJ and AJ integrity. In sham-iECKO mice compared to sham-littermates, the detailed quantitative analysis in extracted brain vessel lysates showed a significant increase of Occludin and Claudin5 levels in iECKO membrane vessel fractions but no obvious differences of Ve cadherin, β catenin expressions (Fig. S6 (a) and (b)). At 14 days after GCAS, Occludin and Claudin5 levels at the membrane were not significantly increased in iECKO vs littermate brain vessel lysates (Figure 4(n) and (o)). These results indicate that the absence of *Pdzrn3* or of its downstream activation signalling might protect against vessel leakage by

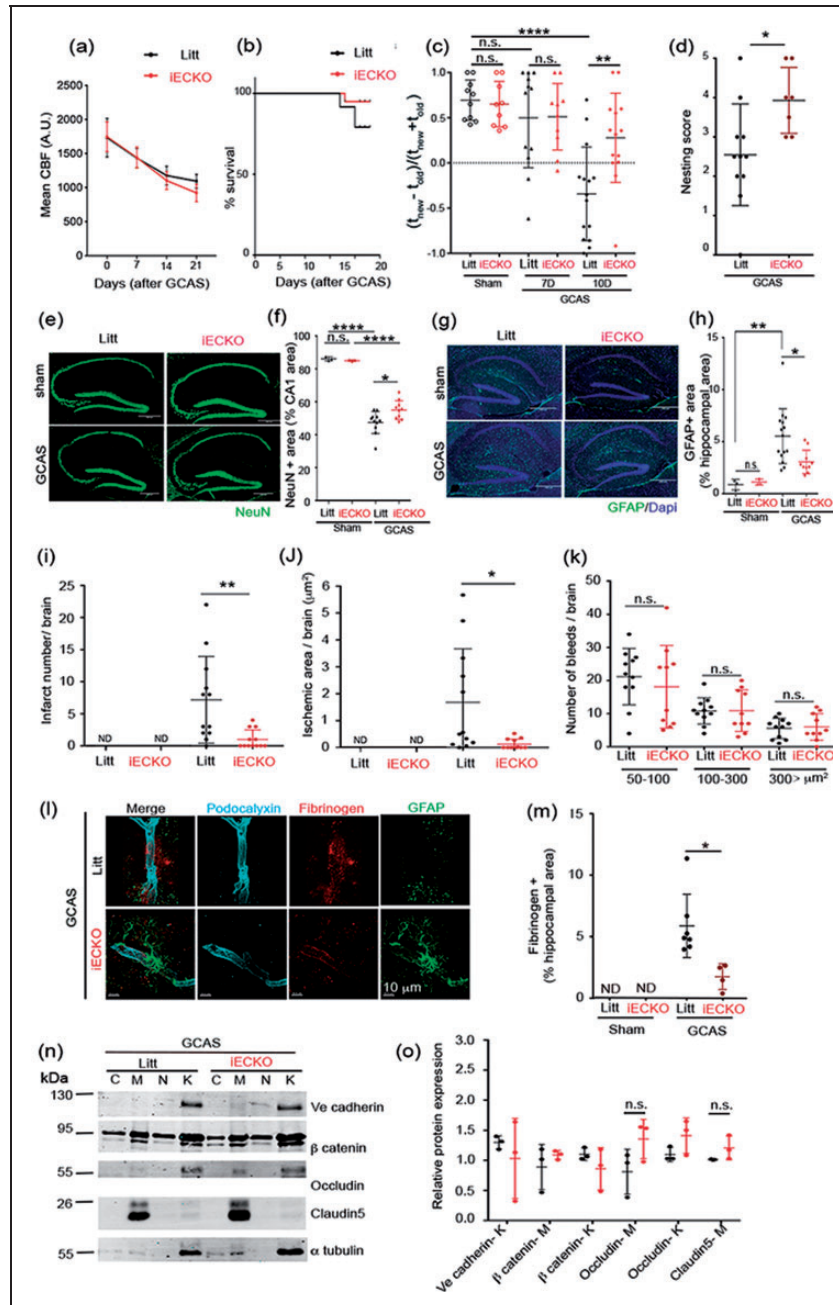


Figure 4. Endothelial *Pdzrn3* depletion protects against cognitive defects, brain damage and vascular leakage after gradual carotid artery stenosis (GCAS). (a) Cerebral blood flow (CBF) decreases gradually in all groups (Littermates, *Pdzrn3* iECKO) after implantation of ameroid constrictors (GCAS). (b) Kaplan-Meier curve showing survival rate of control and *Pdzrn3* iECKO (iECKOE) mice before and until 21 days after GCAS ($n = 10$ to 13 per group). (c) Spatial novelty preference in Y-maze after GCAS evaluated before (sham), after GCAS at 7 days and at 10 days showing that endothelial deletion of *Pdzrn3* (iECKO) protects against chronic hypoperfusion-induced loss of cognitive functions. Each group contained 9–14 mice and each mouse is indicated as a dot in graphs. Data are represented as individual values plus means \pm SD. Significance was assessed by 2-way ANOVA. (d) nesting score of littermate and iECKO mice after 10 days of GCAS. $n = 7$ –10 mice/group. Bars indicate mean \pm s.e.m. Mann-Whitney test was performed. $*p < 0.05$. (e) Representative hippocampal immunofluorescent staining for NeuN from non-operated littermate (Sham) and after GCAS at 21 days in littermate, iECKO mice. (f) NeuN+ cells were quantified as a percentage of the area occupied in the CA1 area non-operated (sham) and after GCAS from iECKO vs their respective littermate mice. (g) representative hippocampal immunohistochemical staining and (h) quantification for GFAP before (sham) and at 21 days after GCAS in littermate and iECKO mice. Data shown in the graphs are obtained in sham condition, from 3 mice per group; in GCAS condition, from $n = 10$ iECKO vs $n = 11$ littermate mice. Data for four brain slices per mouse were

Continued.

strengthening endothelial tight junctions under ischemic challenge.

Overall, endothelial *Pdzn3* overexpression produces phenotypes opposite to those of endothelial *Pdzn3*-deleted mice suggesting that PDZRN3-induced signaling tightly regulates barrier maintenance.

Endothelial *Pdzn3* depletion protects against cognitive impairment, enhancing the strength of the BBB with reduced IgG leakage in a mouse model of AD

BBB disruption is detected in early AD and correlates with disease progression.³⁹ We examined whether targeting endothelial *Pdzn3* may reduce BBB disruption in AD pathology. To test this hypothesis, we crossed APPSwe/PSEN1dE9 mouse (APP/PS1) with transgenic *Pdgfb-Cre^{ERT2}; Pdzn3^{fl/fl}* to generate AD mouse cohorts with EC specific depletion of *Pdzn3* (APP/PS1; iECKO) and their littermate control (APP/PS1; Litt) and their respective non dementia (ND) littermate groups (ND-iECKO and ND-litt controls). We confirmed in both APP/PS1; Litt and in APP/PS1; iECKO mouse groups, a reduced cerebral blood flow at the age of 6 months which worsened at 12 months of age with no difference in between the groups (Figure 5(a)). We tested the effects of the endothelial depletion of *Pdzn3* on cognitive impairment from 6 to 10 months of age by using a Y-maze test as reported above. We compared spatial recognition memory in ND (Litt and iECKO) groups, versus APP/PS1 (Litt and iECKO) groups in age matched groups. At 6-months of age, no differences were observed but strikingly, at 8 months and 10 months, APP/PS1; Litt mice were severely impaired in the spatial recognition memory paradigm whereas APP/PS1; iECKO littermates performed as well as 6 to 10-months-old ND- litt control and ND- iECKO mice (Figure 5(b)). We used a complimentary assay as AD leads to impairment of activities of daily living such as nesting.⁴⁰ In agreement, we reported that singly housed APP/PS1; Litt male built significantly poorer nests at 8-months of

age compared to their ND littermate groups whereas APP/PS1; iECKO group were able to construct nest as efficiently as ND littermate groups (Figure 5(c)).

Analysis of APP/PS1 brain sections showed a significant increase of IgG extravasation from young adulthood (6 months of age) to middle age (12 months of age) in cortex (Fig. 6(d)) and in hippocampus (Fig S9 (a)). Notably, in APP/PS1 littermate cortical sections, we observed large areas of IgG deposit which correlated with NeuN-negative cell nuclei at the age of 12 months. In contrast, there was no such IgG positive/NeuN-negative large areas in the cortex of APP/PS1; iECKO mice (Figure 5(d) to (f)). In hippocampus region, we found similar effects: while IgG leakage was increased both at 6 and 12 months, it was reduced significantly at 6 months in the hippocampus of APP/PS1; iECKO mice compared to their littermates (Fig S9 (a,c)), both APP/PS1; Litt and APP/PS1; iECKO mice exhibited a reduced neuronal loss in the CA1 hippocampal region at 12 months (Fig S9 (a, b)),

We reported an increase of GFAP and Iba1 immunolabeling at 6 months in both APP/PS1; Litt and APP/PS1; iECKO in the cortex but not in the hippocampus; this activation is amplified at 12 months in APP/PS1; Litt but not in APP/PS1; iECKO cortical and hippocampal areas of brains (Figure 5(d) to (h); Fig S9 (a, d, e)). These findings suggest that increase IgG deposits in APP/PS1; Litt group leads to increase activation of astrocytes while in APP/PS1; iECKO, deletion of *Pdzn3* in EC in reducing endothelial permeability protects against astrogliosis.

Reduced BBB breakdown in APP/PS1 with endothelial-specific depletion of *Pdzn3* (iECKO) with enhanced expression levels of wnt target gene and of tight junction proteins in brain vessels

Given the significant increase in vascular permeability of APP/PS1 mice,⁴⁷ and given the role of Wnt/ β catenin in the maintain of BBB stability,⁴¹ we wanted to understand if Wnt pathway was affected under APP/PS1 phenotype at the NVU level. To this end, brain vessel

Figure 4. Continued

recorded and averaged to produce a single value for each mouse. Two-way ANOVA was performed. Data are represented as individual values plus means \pm SD. (i) Infarct number, (j) ischemic area, and (k) bleed number were quantified. Quantifications were done in brains from either non operated (sham) or after 21 days of GCAS littermates (litt) vs *Pdzn3* iECKO mice. Each group contained 10-12 mice and each mouse is indicated as a dot in graphs. (l) Representative confocal images reconstructed in 3D of hippocampal vessels co-immunolabelled with Podocalyxin (light blue) Fibrinogen (red) and GFAP (green) from iECKO vs littermate mice after 14 days of GCAS showing fibrinogen leakage. Scale bar represents 10 μ m. (m) Fibrinogen release was quantified as a percentage of the area occupied in hippocampal region after GCAS from *Pdzn3* iECKO (n = 4) versus littermates (n = 7) mice at 14 days after GCAS. Data are presented as mean \pm SD. Unpaired t-test was performed. *P \leq 0.05. (n) Representative immunoblot images and quantification (o) of TJ proteins Occludin, Claudin5, AJ protein Ve cadherin and of β catenin in subcellular brain microvessel fractions in non operated (sham) at 14 days after GCAS from littermate and *Pdzn3* iECKO mice: cytosol (C), Membrane (M), nucleus (N), cytoskeleton (K). n = 3. Data are represented as mean \pm SD. Mann-Whitney test was performed. *p < 0.05.

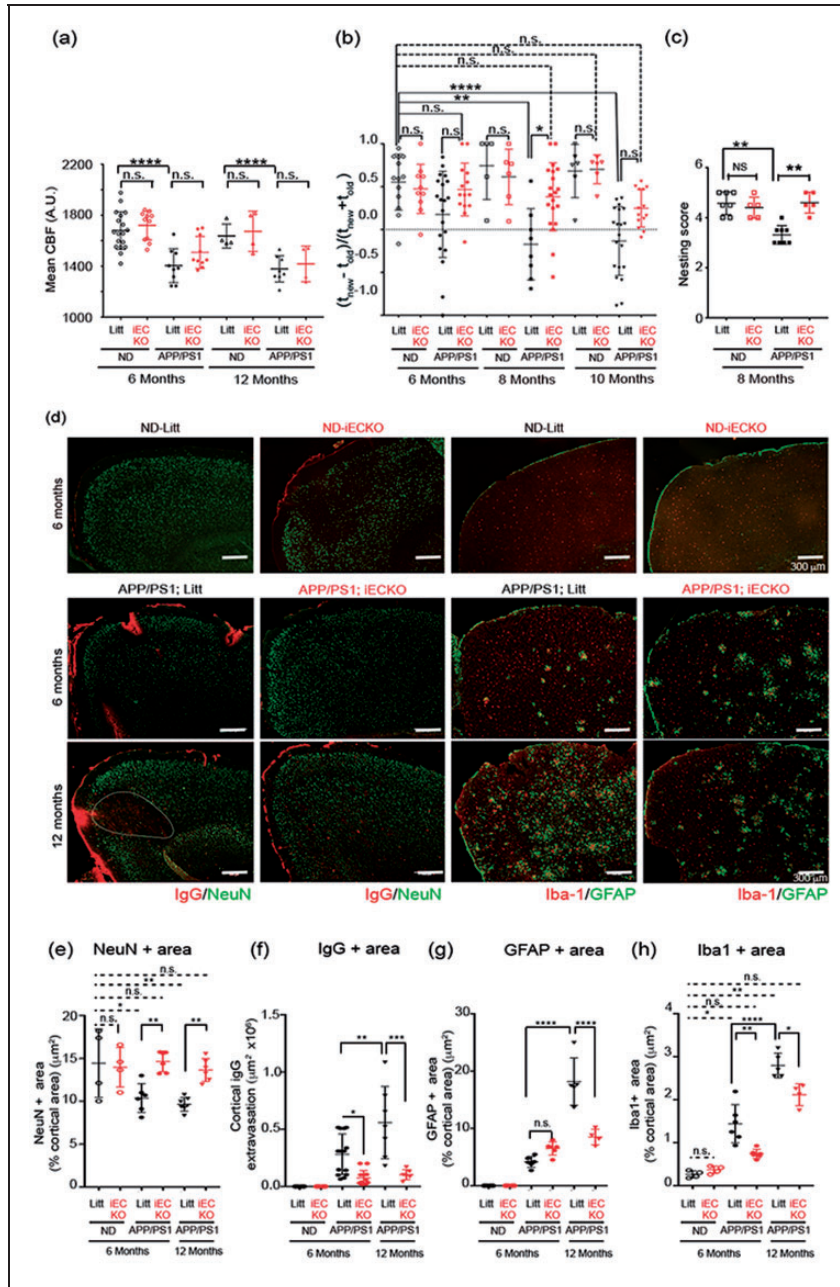


Figure 5. Endothelial *Pdzrn3* depletion protects against cognitive impairment, limiting BBB leakage in a mouse model of AD.

(a) Cerebral cortical blood flow (CBF) decreases at 6 months ($n = 10-18$ mice per group) and 12 months ($n = 4-11$ mice per group) in APP/PS1 groups (APP/PS1; iECKO vs APP/PS1; Litt) vs non demented (ND) groups (age-matched iECKO vs littermate groups respectively ND-iECKO vs ND-litt). Each point represents a different mouse. Data are represented as individual values plus means \pm SD. (b) Y-maze exploration test: deletion of *Pdzrn3* (iECKO) protects against AD-induced loss of spatial novelty preference in Y-maze evaluated in APP/PS1; iECKO vs APP/PS1 mice groups at 6, 8 and 10 months of age ($n = 14-20$ mice per group) vs non demented (ND) groups (age-matched iECKO vs littermate groups respectively ND-iECKO vs ND-litt) ($n = 6-13$ mice per group). Each point represents a different mouse. Data are presented as mean \pm SD. Two-way ANOVA was performed. (c) nesting score of 8 month-old ND; litt and iECKO mice and APP/PS1; litt and iECKO mice. $n = 5-8$ mice. Student's t-test. $*P < 0.05$. Data are represented as individual values plus means \pm SD. Immunostaining of representative cortical brain section images stained for (d) IgG (red) and NeuN (green) and for Iba1 (red) and GFAP (green) in APP/PS1; iECKO vs their age-matched littermates APP/PS1; Litt at 6 and 12 months and non demented (ND) iECKO vs their age-matched littermate groups at 6 months. Scale bar represents 300 μm . (e) NeuN, (f) IgG (g) GFAP and (h) Iba1 + area were quantified as a percentage of the area occupied in cortical region. Each point represents a different mouse. Data are represented as individual values plus means \pm SD. $n = 6-14$ mice/APP/PS1 group at 6 months; $n = 4-7$ mice/APP/PS1 group at 12 months; $n = 4$ mice/ND groups. One-way ANOVA was performed.

fragments were harvested from 8 months old APP/PS1 versus ND mice and we analyzed the expression of Wnt/ β catenin related target genes by quantitative real-time PCR (qRT-PCR). APP/PS1; Litt mice showed significantly lower expression levels of several Wnt/ β catenin target genes as *Lef1*, *Axin2*, *Gpr124* and *Nkd1* (Figure 6(a)). These data are in support of a vascular AD hypothesis involving a premature dysfunction of endothelial cell barrier at the NVU. As *Pdzn3* iECKO reduced APP/PS1 vessel permeability, we further analyzed the transcriptional expression of Wnt/ β catenin related genes at 8 months of age in ND- and APP/PS1 mouse groups. We found a maintain of the expression of Wnt/ β catenin target genes in APP/PS1; iECKO mice compared to APP/PS1; Litt mice, suggesting that endothelial depletion of *Pdzn3* protects BBB against precocious dysfunction.

The expression and the localization of EC junctional proteins were then analyzed by Western blot analysis. We observed that endothelial depletion of *Pdzn3* induced an enrichment of Occludin in both skeletal and membrane fractions and of Claudin 5 in membrane fractions by densitometric analysis in lysates from brain vessels extracted of 8 months old littermates both APP/PS1; iECKO mutant vs APP/PS1; Litt mice and ND-iECKO mutant vs ND; litt mice (Figure 6(b) to (c)). Confocal microscopy was used to characterize patterns of Claudin 5 expression at EC junctions on isolated SMA negative-capillaries. In line with previous finding, we confirmed that Claudin5 was more abundant into EC-EC contact sites in brain microvessels from APP/PS1; iECKO mice than in APP/PS1; Litt control mice and in ND-iECKO mutant vs ND; litt mice (Figure 6(d) to (e)). The distribution and the expression levels of Ve cadherin was not modified in capillaries from APP/PS1; iECKO vs APP/PS1; Litt mice but increased in ND; iECKO vs ND; Litt. These data suggest that down regulation of endothelial PDZRN3 signaling leads to increase BBB strength by sustaining endothelial tight junction strands.

Discussion

In the present study, we provide a molecular link between loss of BBB integrity and the cognitive decline under GCAS and AD pathologies. We report that under the stress of GCAS, forced expression of *Pdzn3* in EC exacerbates BBB breakdown and vascular damage combined with a precocious alteration of cognitive functions. In contrast, blocking *Pdzn3* expression in the adult brain endothelium increases tight junction expression, and limits lesion-induced BBB leakage. We evidence that this protective effect translated into reduced tissue damage (neuronal loss,

reactive astrocytes, microinfarcts). Overall, EC *Pdzn3* loss of function drastically limits cognitive impairment evolution in GCAS and AD models. These data highlight a key role of endothelial *Pdzn3* signaling in controlling integrity of the neurovascular unit.

Mice were subjected to GCAS to reduce gradually brain perfusion as it relates to VCI pathologies; this germane model was shown to induce vascular damage and cognitive dysfunction.^{22,23} As demonstrated here, GCAS model displayed hallmarks of human VCI, with an increase of BBB leakage, as testified by an extravasation of fibrinogen and other macromolecules, an increase number of microinfarcts and microbleeds and, a loss of hippocampal CA1 neurons with a strong astrocyte activation. Confocal images showed disruption of endothelial tight junctions and loss of astrocytic end feet layer onto blood brain vessels causing focal breach of the BBB.

Rupture of BBB integrity was shown to be correlated with neural dysfunction and behavioural phenotype.^{6,44} Passage of blood macromolecules in brain parenchyma is highly detrimental for neurons. Experiments reported that albumin infusion directly in cerebral ventricles of rats induced a neural hyperexcitability events.⁴⁵ As demonstrated in AD, accumulation of blood proteins as fibrinogen may enhances brain circulatory dysfunction in binding to soluble, non-fibrillar, amyloid species, forming plasmin-resistant blood clots or may induce demyelination defects, and subsequent cognitive impairment.^{46,47} Under GCAS, we observed, in *Pdzn3* iECKO mice, an induced hyper-permeability with a massive influx of blood macromolecules as fibrinogen or IgG. This exacerbated BBB dysfunction led to an increase of the number and size of infarcts, of the number of microbleeds, a loss of CA1 neurons, an activation of astrocytes in *Pdzn3* iECKO mice compared to their control littermates.

We have previously evidenced that EC specific over-expression of *Pdzn3* led to early embryonic lethality with severe brain hemorrhages and altered organization of endothelial intercellular junctions.²¹ In contrast, endothelial depletion of *Pdzn3* leads to a reduced brain vessel permeability, decrease neurological insults and finally protects against loss of cognitive capacities, in both VCI and AD models. These data are concordant with our previous reports showing that endothelial-specific loss of *Pdzn3* prevented vascular leakage in a mouse model of transient ischemic stroke²¹. Overall, we showed that controlling vascular damage at the BBB correlated with cognitive function, in accordance with recent reports showing that BBB dysfunction is directly causative for the neuronal phenotype.⁴ Therefore, these data underline that in adult, endothelial *Pdzn3* signaling needs to be finely regulated to maintain the integrity of brain vasculature.

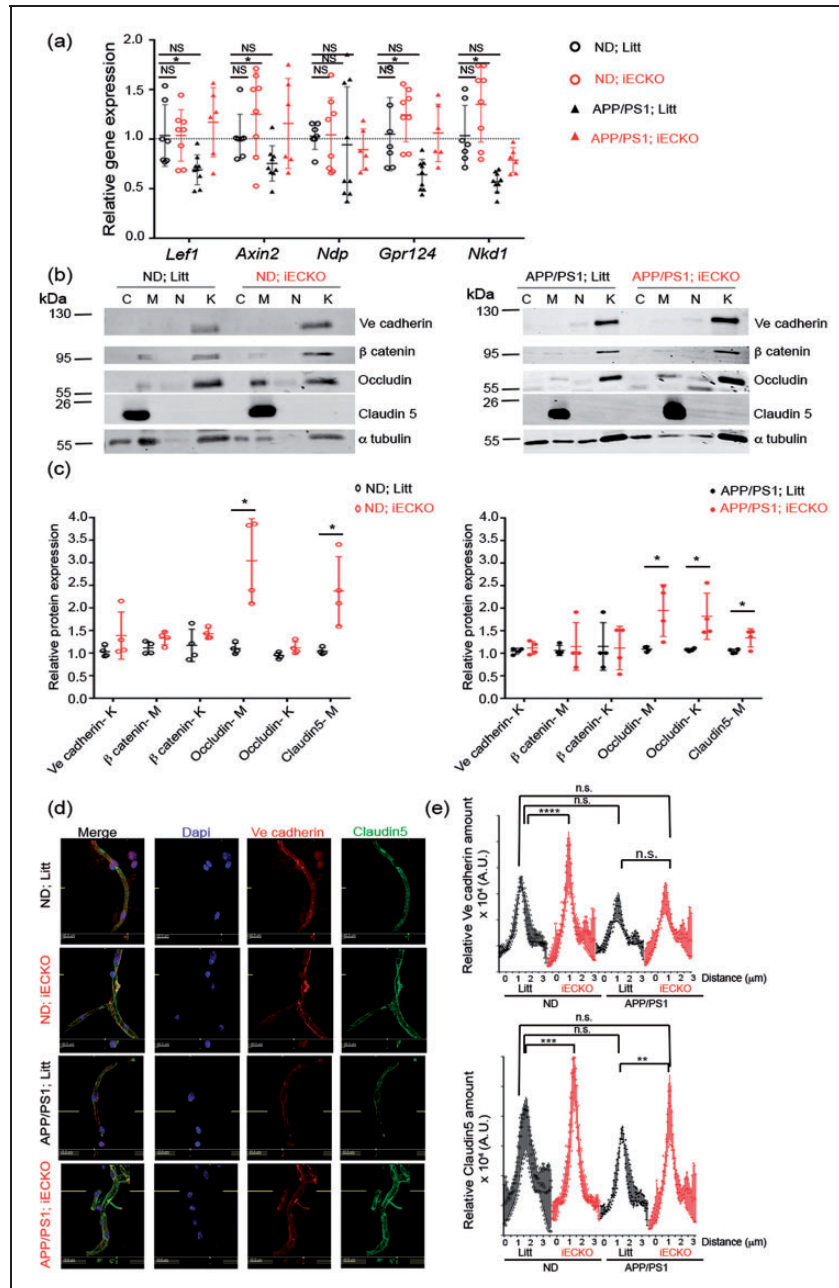


Figure 6. Wnt target genes and tight junction proteins are enhanced in vessel fragments from APP/PS1-iECKO mice. (a) Transcript levels in brain capillaries isolated from either non-demented iECKO (ND-iECKO) vs non-demented littermates (ND-litt) and APP/PS1; iECKO vs APP/PS1; Litt mice. Data are normalized to that of *Pecam* and presented as the relative fold to ND-litt. Mann-Whitney test was performed. *p < 0.05. (b) Representative immunoblot images and (c) quantification of TJ proteins Occludin, Claudin5, AJ protein Ve cadherin and of β catenin in subcellular brain microvessel fractions from ND; Litt vs ND; iECKO (n = 3) and APP/PS1; Litt vs APP/PS1; iECKO mice (n = 4). Cytosol (C), Membrane (M), nucleus (N), cytoskeleton (K) (n = 4). Data are represented as mean \pm SD. One-way ANOVA was performed. *p < 0.05. (d) Representative immunostaining of isolated capillaries for Ve Cadherin (green) and Claudin5 (red) from ND; Litt vs ND; iECKO and APP/PS1; Litt vs APP/PS1; iECKO brains at 6 months of age. (e) Ve cadherin and Claudin5 expression was semi quantified at cell-cell contacts by measuring fluorescence intensity in capillaries isolated from brains from 3 groups (ND and APP/PS1; littermates and iECKO). Fluorescence intensity profile curve per cell was then plotted. Bars denote mean \pm SD; ≥ 10 vessels from three independent experiments. Two-way ANOVA was performed. n.s., not significant; ***p < 0.001; ****p < 0.0001.

Concerning the mechanism of vascular permeability, we analyzed EC adherens and tight junction expressions in vessel extracts. *Pdzrn3* iECOEC brain vessel revealed a discrete decrease of Claudin5 expression levels at the cell membrane but not significant alteration in other markers as Ve cadherin, and Occludin. Under GCAS insult, iECOEC mutants displayed leaky vessels with a dramatic loss of claudin5 and occludin at the cell membranes. Conversely, EC depletion of *Pdzrn3* led to an enrichment of Occludin and Claudin 5 either in sham conditions and in AD models. It was reported that knockout of genes encoding specific TJ components as occludin⁴⁹ and ZO1⁵⁰ proteins did not show gross TJ permeability. Claudin 5 plays a major role for TJ formation and maintain, linked to the cytoskeleton by zonula occludens family protein members as ZO1. Deletion of the *Cldn5* gene in mice increases, postnatally, the paracellular permeability of the BBB to small molecules⁵¹ but does not cause the junctions to break. In adult mice, the deletion of *Cldn5* leads to convulsion problems and ultimately to death.⁵² It is proposed that the presence of other members of claudins (notably Claudins 11, 12 and 25) would allow the maintenance of joint structures.⁵³ Then, it may be necessary to have a coordinated downregulation of several TJ components to enhance TJ permeability.

Vascular contributions to cognitive impairment are increasingly recognized in AD, as shown by neuropathological, neuroimaging, and cerebrospinal fluid biomarker studies.^{9,39,54} AD patients display cerebral blood flow reductions, loss of vascular integrity and blood brain barrier (BBB) disruption.^{2,5-7} In line, in AD mouse model, BBB leakage with microglia activation⁵⁶⁻⁵⁸ and a decrease of the CBF worsened the severity of the pathology. Interestingly, it was shown that mechanisms of autoregulation of BBB permeability via a transient decrease of both Claudin5 and Occludin may enhance diffusion of A β (1-40) monomers across BBB⁶⁰ underlying the functional role of BBB in amyloid fragment clearance. Here, we reported that, endothelial *Pdzrn3* depletion when combined with APP/PS1 overexpression, leads to reduce astrocyte activation. This effect is correlated with a reduction of BBB leakage and an enhancement of TJ proteins in vessel fragments which may be protective for neural tissue.

Several groups have reported that the Wnt/ β catenin signaling pathway is required for the integrity and maintenance of the properties of BBB.^{12,16,61,62} It was shown to regulate Claudin5 levels in endothelium. Recent work highlighted the importance of the Wnt pathway in the plasticity of CE. The choroid plexuses are highly vascularized epithelial tissues responsible for the production of most of the cerebrospinal fluid that circulates throughout the ventricular system of the brain. The capillaries of the choroid plexus have no

BBB properties; they are fenestrated and permeable with a reduced expression of Claudin5. The canonical Wnt pathway was shown poorly active in these structures. The activation of the canonical Wnt pathway in choroids ECs would reverse their phenotype; they may then acquire BBB properties with an increase in expression of Claudin5^{12,16} Recently, an elegant study demonstrated that astrocytic Wnt release is crucial for BBB integrity; depletion of Wnt ligands was correlated with edema formation and increased vascular tracer leakage in adult brain.⁶⁴ In isolated microvessels from adult iECOEC mice, we reported a downregulation of a Wnt target gene *Axin2* as compared to microvessels from littermate, indicating of reduced Wnt canonical signaling. We reported then that few Wnt canonical target genes (*Lef1*, *Axin2*, *Gpr124*, *Nkd1*) are downregulated at the BBB level in APP/PS1 mouse mutants but not in APP/PS1; iECKO. It would be tempting to speculate that the *Pdzrn3* signaling pathway in EC may impair the activation of the canonical Wnt/ β -catenin pathway at the BBB to favor its destabilization in VCI and AD pathological models.

Funding

The author(s) disclosed receipt of the following financial support for the research, authorship, and/or publication of this article: Agence Nationale de la Recherche Grant ANR 16-CE17-0001-01. Institut National de la Santé et de la Recherche Médicale. University of Bordeaux. This work is supported by a grant overseen by the French National Research Agency (ANR) as part of the "Investissements d'Avenir" Program ANR-18-RHUS-002 and as part of the "ERA-CVD" Program ANR-20-ECVD-0002-01 (ANR / ENRICH).

Acknowledgements

We thank Jeremy Teillon for iDISCO immunolabeling and image analysis, Sylvain Grolleau and Maxime David for their technical help.

Declaration of conflicting interests


The author(s) declared no potential conflicts of interest with respect to the research, authorship, and/or publication of this article.

Authors' contributions

Conceptualization: FG, TC, CD
 Methodology: FG, AA, SR, PB, CP, JT, JLM, BB
 Funding acquisition: TC, CD
 Writing – original draft: TC, CD
 Writing – review & editing: JLM, BB, PD, TC, CD

Data and materials availability

All data are available in the main text or the supplementary materials.

ORCID iDsJean Luc Morel  <https://orcid.org/0000-0001-8079-6851>Cecile Dupl a  <https://orcid.org/0000-0001-8003-3969>**Supplemental material**

Supplemental material for this article is available online.

References

- Iadecola C, Duering M, Hachinski V, et al. Vascular cognitive impairment and dementia. *J Am Coll Cardiol* 2019; 73: 3326–3344.
- Sweeney MD, Montagne A, Sagare AP, et al. Vascular dysfunction – the disregarded partner of Alzheimer’s disease. *Alzheimers Dement* 2019; 15: 158–167.
- Snyder HM, Corriveau RA, Craft S, et al. Vascular contributions to cognitive impairment and dementia including Alzheimer’s disease. *Alzheimers Dement* 2015; 11: 710–717.
- Sweeney MD, Sagare AP and Zlokovic BV. Blood–brain barrier breakdown in Alzheimer disease and other neurodegenerative disorders. *Nat Rev Neurol* 2018; 14: 133–150.
- Gottesman RF, Schneider ALC, Zhou Y, et al. Association between midlife vascular risk factors and estimated brain amyloid deposition. *JAMA* 2017; 317: 1443–1450.
- Nation DA, Sweeney MD, Montagne A, et al. Blood–brain barrier breakdown is an early biomarker of human cognitive dysfunction. *Nat Med* 2019; 25: 270–276.
- Arvanitakis Z, Capuano AW, Leurgans SE, et al. Relation of cerebral vessel disease to Alzheimer’s disease dementia and cognitive function in elderly people: A cross-sectional study. *Lancet Neurol* 2016; 15: 934–943.
- van de Haar HJ, Jansen JFA, van Osch MJP, et al. Neurovascular unit impairment in early Alzheimer’s disease measured with magnetic resonance imaging. *Neurobiol Aging* 2016; 45: 190–196.
- Iturria-Medina Y, Sotero RC, Toussaint PJ et al.; Alzheimer’s Disease Neuroimaging Initiative. Early role of vascular dysregulation on late-onset Alzheimer’s disease based on multifactorial data-driven analysis. *Nat Commun* 2016; 7: 11934.
- Iadecola C. The neurovascular unit coming of age: a journey through neurovascular coupling in health and disease. *Neuron* 2017; 96: 17–42.
- Daneman R and Prat A. The blood–brain barrier. *Cold Spring Harb Perspect Biol* 2015; 7: a020412.
- Liebner S, Corada M, Bangsow T, et al. Wnt/beta-catenin signaling controls development of the blood–brain barrier. *J Cell Biol* 2008; 183: 409–417.
- Stenman JM, Rajagopal J, Carroll TJ, et al. Canonical wnt signaling regulates organ-specific assembly and differentiation of CNS vasculature. *Science* 2008; 322: 1247–1250.
- Daneman R, Agalliu D, Zhou L, et al. Wnt/-catenin signaling is required for CNS, but not non-CNS, angiogenesis. *Proc Natl Acad Sci USA* 2009; 106: 641–646.
- Wang Y, Rattner A, Zhou Y, et al. Norrin/Frizzled4 signaling in retinal vascular development and blood brain barrier plasticity. *Cell* 2012; 151: 1332–1344.
- Wang Y, Sabbagh MF, Gu X, et al. Beta-catenin signaling regulates barrier-specific gene expression in circumventricular organ and ocular vasculatures. *eLife* 2019; 8: 3221. DOI: 10.7554/eLife.43257.
- Posokhova E, Shukla A, Seaman S, et al. GPR124 functions as a WNT7-Specific coactivator of canonical β -catenin signaling. *Cell Rep* 2015; 10: 123–130.
- Benz F, Wichitnaowarat V, Lehmann M, et al. Low wnt/ β -catenin signaling determines leaky vessels in the subfornical organ and affects water homeostasis in mice. *eLife* April 2019; 8. Epub ahead of print 1 DOI: 10.7554/eLife.43818.
- Jambusaria A, Klomp J, Hong Z, et al. A computational approach to identify cellular heterogeneity and tissue-specific gene regulatory networks. *BMC Bioinformatics* December 2018; 19: 217. Epub ahead of print DOI: 10.1186/s12859-018-2190-6.
- Sewduth RN, Jaspard-Vinassa B, Peghaire C, et al. The ubiquitin ligase PDZRN3 is required for vascular morphogenesis through wnt/planar cell polarity signalling. *Nat Commun* 2014; 5: 4832.
- Sewduth RN, Kovacic H, Jaspard-Vinassa B, et al. PDZRN3 destabilizes endothelial cell-cell junctions through a PKCzeta-containing polarity complex to increase vascular permeability. *Science Signaling* January 2017; 10. Epub ahead of print 31 DOI: 10.1126/scisignal.aag3209.
- Hattori Y, Kitamura A, Nagatsuka K, et al. A novel mouse model of ischemic carotid artery disease. *PLoS ONE* 2014; 9: e100257.
- Hattori Y, Enmi J, Iguchi S, et al. Gradual carotid artery stenosis in mice closely replicates hypoperfusive vascular dementia in humans. *JAHA*; 5. Epub Ahead of Print 23 February 2016; DOI: 10.1161/JAHA.115.002757.
- Percie Du Sert N, Hurst V, Ahluwalia A, et al. The ARRIVE guidelines 2.0: updated guidelines for reporting animal research. *J Cereb Blood Flow Metab* 2020; 40: 1769–1777.
- Claxton S, Kostourou V, Jadeja S, et al. Efficient, inducible cre-recombinase activation in vascular endothelium. *Genesis* 2008; 46: 74–80.
- Mora P, Hollier P-L, Guimbal S, et al. Blood–brain barrier genetic disruption leads to protective barrier formation at the glia limitans. *PLoS Biol* 2020; 18: e3000946.
- Guillabert-Gourgues A, Jaspard-Vinassa B, Bats ML, et al. Kif26b controls endothelial cell polarity through the dishevelled/Daam1-dependent planar cell polarity-signaling pathway. *Mol Biol Cell* 2016; 27: 941–953.
- Deacon RM. Assessing nest building in mice. *Nat Protoc* 2006; 1: 1117–1119.
- Liu Q, Radwanski R, Babadjouni R, et al. Experimental chronic cerebral hypoperfusion results in decreased pericyte coverage and increased blood–brain barrier

- permeability in the corpus callosum. *J Cereb Blood Flow Metab* 2019; 39: 240–250.
30. Wang L, Sharma K, Deng H-X, et al. Restricted expression of mutant SOD1 in spinal motor neurons and interneurons induces motor neuron pathology. *Neurobiol Dis* 2008; 29: 400–408.
 31. Coelho-Santos V and Shih AY. Postnatal development of cerebrovascular structure and the neuroglial unit. *Wiley Interdiscip Rev Dev Biol* March 2020; 9: e363. Epub ahead of print DOI: 10.1002/wdev.363.
 32. Boulay A-C, Saubaméa B, Declèves X, et al. Purification of mouse brain vessels. *J Vis Exp* 2015; 10: e53208.
 33. Holland PR, Searcy JL, Salvadores N, et al. Gliovascular disruption and cognitive deficits in a mouse model with features of small vessel disease. *J Cereb Blood Flow Metab* 2015; 35: 1005–1014.
 34. Shang J, Yamashita T, Zhai Y, et al. Strong impact of chronic cerebral hypoperfusion on neurovascular unit, cerebrovascular remodeling, and neurovascular trophic coupling in Alzheimer's disease model mouse. *J Alzheimers Dis* 2016; 52: 113–126.
 35. Li H, Zhang N, Lin H-Y, et al. Histological, cellular and behavioral assessments of stroke outcomes after photothrombosis-induced ischemia in adult mice. *BMC Neurosci* 2014; 15: 58.
 36. Roberts JM, Maniskas ME and Bix GJ. Bilateral carotid artery stenosis causes unexpected early changes in brain extracellular matrix and blood-brain barrier integrity in mice. *PLoS ONE* 2018; 13: e0195765.
 37. Liu S, Grigoryan MM, Vasilevko V, et al. Comparative analysis of H&E and Prussian blue staining in a mouse model of cerebral microbleeds. *J Histochem Cytochem* 2014; 62: 767–773.
 38. Montagne A, Zhao Z and Zlokovic BV. Alzheimer's disease: a matter of blood-brain barrier dysfunction? *J Exp Med* 2017; 214: 3151–3169.
 39. Filali M, Lalonde R and Rivest S. Cognitive and non-cognitive behaviors in an APPswe/PS1 bigenic model of Alzheimer's disease. *Genes Brain Behav* 2009; 8: 143–148.
 40. Zhou Y, Wang Y, Tischfield M, et al. Canonical WNT signaling components in vascular development and barrier formation. *J Clin Invest* 2014; 124: 3825–3846.
 41. Tomkins O, Kaufer D, Korn A, et al. Frequent blood-brain barrier disruption in the human cerebral cortex. *Cell Mol Neurobiol* 2001; 21: 675–691.
 42. Milikovsky DZ, Ofer J, Senatorov VV, et al. Paroxysmal slow cortical activity in Alzheimer's disease and epilepsy is associated with blood-brain barrier dysfunction. *Sci Transl Med* 2019; 11(521): eaaw8954.
 43. Ryu JK, Petersen MA, Murray SG, et al. Blood coagulation protein fibrinogen promotes autoimmunity and demyelination via chemokine release and antigen presentation. *Nat Commun* 2015; 6: 8164.
 44. Merlini M, Rafalski VA, Rios Coronado PE, et al. Fibrinogen induces microglia-mediated spine elimination and cognitive impairment in an Alzheimer's disease model. *Neuron* 2019; 101: 1099–1108.e6.
 45. Saitou M, Furuse M, Sasaki H, et al. Complex phenotype of mice lacking occludin, a component of tight junction strands. *Mol Biol Cell* 2000; 11: 4131–4142.
 46. Katsuno T, Umeda K, Matsui T, et al. Deficiency of zonula occludens-1 causes embryonic lethal phenotype associated with defected yolk sac angiogenesis and apoptosis of embryonic cells. *Mol Biol Cell* 2008; 19: 2465–2475.
 47. Merlini M, Rafalski VA, Rios Coronado PE, et al. Fibrinogen induces microglia-mediated spine elimination and cognitive impairment in an Alzheimer's disease model. *Neuron* 2019; 101: 1099–1108.e6.
 48. Nitta T, Hata M, Gotoh S, et al. Size-selective loosening of the blood-brain barrier in claudin-5-deficient mice. *J Cell Biol* 2003; 161: 653–660.
 49. Greene C, Kealy J, Humphries MM, et al. Dose-dependent expression of claudin-5 is a modifying factor in schizophrenia. *Mol Psychiatry* 2018; 23: 2156–2166.
 50. Berndt P, Winkler L, Cording J, et al. Tight junction proteins at the blood-brain barrier: far more than claudin-5. *Cell Mol Life Sci* 2019; 76: 1987–2002.
 51. Zenaro E, Piacentino G and Constantin G. The blood-brain barrier in Alzheimer's disease. *Neurobiol Dis* 2017; 107: 41–56.
 52. Ryu JK and McLarnon JG. A leaky blood-brain barrier, fibrinogen infiltration and microglial reactivity in inflamed Alzheimer's disease brain. *J Cell Mol Med* 2009; 13: 2911–2925.
 53. Zipsper BD, Johanson CE, Gonzalez L, et al. Microvascular injury and blood-brain barrier leakage in Alzheimer's disease. *Neurobiol Aging* 2007; 28: 977–986.
 54. Adams RA, Passino M, Sachs BD, et al. Fibrin mechanisms and functions in nervous system pathology. *Mol Interv* 2004; 4: 163–176.
 55. Keaney J, Walsh DM, O'Malley T, et al. Autoregulated paracellular clearance of amyloid- β across the blood-brain barrier. *Sci Adv* 2015; 1: e1500472.
 56. Wang Y, Cho C, Williams J, et al. Interplay of the norrin and Wnt7a/Wnt7b signaling systems in blood-brain barrier and blood-retina barrier development and maintenance. *Proc Natl Acad Sci U S A* 2018; 115: E11827–E11836. USA
 57. Liu L, Wan W, Xia S, et al. Dysfunctional wnt/ β -catenin signaling contributes to blood-brain barrier breakdown in Alzheimer's disease. *Neurochem Int* 2014; 75: 19–25.
 58. Guérit S, Fidan E, Macas J, et al. Astrocyte-derived wnt growth factors are required for endothelial blood-brain barrier maintenance. *Prog Neurobiol* 2021; 199: 101937.